Tunable Arrays of ZnO Nanorods and Nanoneedles via Seed Layer and Solution Chemistry

ARTICLE *in* CRYSTAL GROWTH & DESIGN · MAY 2008

Impact Factor: 4.89 · DOI: 10.1021/cg800052p

7 AUTHORS, INCLUDING:

Yun-Ju Lee
University of Texas at Dallas
60 PUBLICATIONS **1,797** CITATIONS

SEE PROFILE

Weihua Hsu
Samsung
768 PUBLICATIONS **20,542** CITATIONS

SEE PROFILE

CRYSTAL GROWTH & DESIGN
2008
VOL. 8, NO. 6
2036–2040

Tunable Arrays of ZnO Nanorods and Nanoneedles via Seed Layer and Solution Chemistry

Yun-Ju Lee,* Thomas L. Sounart,† Jun Liu,‡ Erik D. Spoerke, Bonnie B. McKenzie, Julia W. P. Hsu, and James A. Voigt

Sandia National Laboratories, P.O. Box 5800 MS-1082, Albuquerque, New Mexico

Received January 14, 2008

ABSTRACT: We have systematically studied the effect of pH and 1,3-diaminopropane additive concentration on the morphology of ZnO nanorod and nanoneedle arrays grown in aqueous solution using a variety of seed layers. Increase in the growth solution pH from 6.8 to 13.2 resulted in a near doubling of the growth rate in the [0001] direction possibly due to attractive interaction between the zinc species and the growth surface at high pH, leading to nanorod arrays with reduced faceting and higher aspect ratios. Increases in 1,3-diaminopropane concentration initially enhanced and subsequently inhibited growth of tapered ZnO nanoneedles on seed layers consisting of ZnO nanoparticles, oriented ZnO films, or columnar facets of ZnO microrods. The final nanoneedle dimensions, packing density, and alignment were strongly affected by 1,3-diaminopropane concentration and seed layer type, which can be explained in terms of the relative strength of zinc chelation by 1,3-diaminopropane, the areal density of seeds, and other factors. The precise tuning of ZnO crystalline morphology via the control of seeding and growth conditions may be beneficial to many potential applications that require these aligned crystalline nanostructures.

Introduction

ZnO nanorod arrays with tunable alignment and morphology have attracted much recent attention due to the potential for producing optimized nanostructures for energy conversion, catalysis, sensing, and other applications. ZnO exhibits a combination of interesting properties including wide band gap ($E_g = 3.3$ eV), high exciton binding energy (60 meV),[1] high electron mobility (100 $cm^2\ V^{-1}\ s^{-1}$),[2] and piezoelectricity,[3,4] with many potential applications in electronic and optoelectronic devices.[1,5,6] By controlling the reaction conditions during heterogeneous deposition of ZnO from aqueous solutions, tunable nanostructures can be readily fabricated.[7–22] Many researchers have utilized growth solutions with different pHs to deposit ZnO nanorod arrays (NRAs) and nanoneedle arrays (NNAs) with distinct morphologies.[7–17] For example, near neutral growth solutions containing the weak base hexamethylene tetraamine (HMT) generally resulted in nanorods with well-defined $\{10\bar{1}0\}$ facets on both planar[7–11] and patterned[12–14] substrates. Growth solutions containing ammonia with pH from 10 to 10.5 were found to deposit ZnO NNAs with different degrees of alignment.[15,16] Highly basic growth solutions (pH 13 to 14) containing NaOH yielded nanorods with circular cross sections, that is, poorly defined $\{10\bar{1}0\}$ facets.[17] Despite these reports, a systematic study of the effect of solution pH on the growth dynamics and morphologies of ZnO NRAs has not been reported.

In order to control the alignment and morphologies of ZnO NRAs and NNAs, we and other groups have also utilized different seed layers for ZnO deposition.[8,9,11,20] Piezoelectric force microscopy has shown that the ZnO nanorods grow in the [0001] direction in solution.[19] Hence, by controlling the crystallographic orientation of a lattice matched seed layer, for example, ZnO, we can control the alignment of ZnO nanorods. For example, using substrates coated with a submonolayer of ZnO nanoparticles as the seed layers, NRAs with low degree of alignment were fabricated due to the random direction of the <0001> growth axis on the nanoparticle seeds.[8,20] In contrast, using highly oriented ZnO films with <0001> direction perpendicular to the substrate as the seed layers, we and others have demonstrated the growth of vertically aligned ZnO NRAs.[9,11] We have also demonstrated more complex ZnO nanostructures such as higher order branched NNAs using a sequential nucleation and growth process in solutions containing organic molecules such as citric acid and diamines.[20–22] However, a systematic comparison of the ZnO nanostructures grown on different seed layers has not yet been performed. In this report, we present a quantitative analysis on the effects of growth solution pH and the growth modifier 1,3-diaminopropane (DAP) concentration on the crystal growth rate and the resulting morphology of ZnO NRAs and NNAs grown on different seed layers.

Experimental Section

Zinc acetate dihydrate (99.999%, Aldrich), zinc nitrate hexahydrate (Fisher), NaOH (Fisher), DAP (Aldrich), and HMT (Fisher) were used as received. To study the effect of growth solution pH on NRA morphology, we first deposited oriented ZnO films on Si substrates by coating them multiple times with an 5 mM ethanolic solution of zinc acetate dihydrate at a relative humidity of ~35%, followed by conversion to ZnO in a 350 °C furnace.[9,11] We then placed the substrates in solutions with either 25 mM $Zn(NO_3)_2$ and HMT at 92.5 °C ("HMT recipe")[9–11] or 1 mM $Zn(NO_3)_2$ and 90 mM NaOH at 70 °C with stirring ("NaOH recipe")[17] for various amounts of time to grow the ZnO NRAs. To study the effect of DAP concentration ([DAP]) on ZnO NNA morphology, two other types of seed layers were prepared in addition to the oriented ZnO film. For a seed layer of nanoparticles, a cleaned glass slide was briefly dipped in an aqueous suspension of ZnO nanoparticles and allowed to dry.[20] For a seed layer of ZnO microrods with ~1 μm diameter, a cleaned glass slide was first placed in aqueous solution of 20 mM $Zn(NO_3)_2$ and HMT at 60 °C for overnight.[21] After each substrate had been seeded, it was then incubated in an aqueous solution of 20 mM $Zn(NO_3)_2$, 20 mM HMT, and 40 mM to 190 mM DAP at 60 °C for 18 h to grow the NNAs. The dimensions and morphology of the ZnO NRAs and NNAs were characterized by a Zeiss field-emission source scanning electron microscope (SEM). Crystallinity and degree of alignment were

* To whom correspondence should be addressed. Ph: (505) 284-4397. Fax: (505) 844-8985. E-mail: ylee@sandia.gov.
† Current address: Intel Corporation, 4500 Dobson Rd, Chandler, AZ 85248.
‡ Current Address: Pacific Northwest National Laboratory, 902 Battelle Boulevard, K2-50, Box 999, Richland, WA 99352.

10.1021/cg800052p CCC: $40.75
Published on Web 05/20/2008

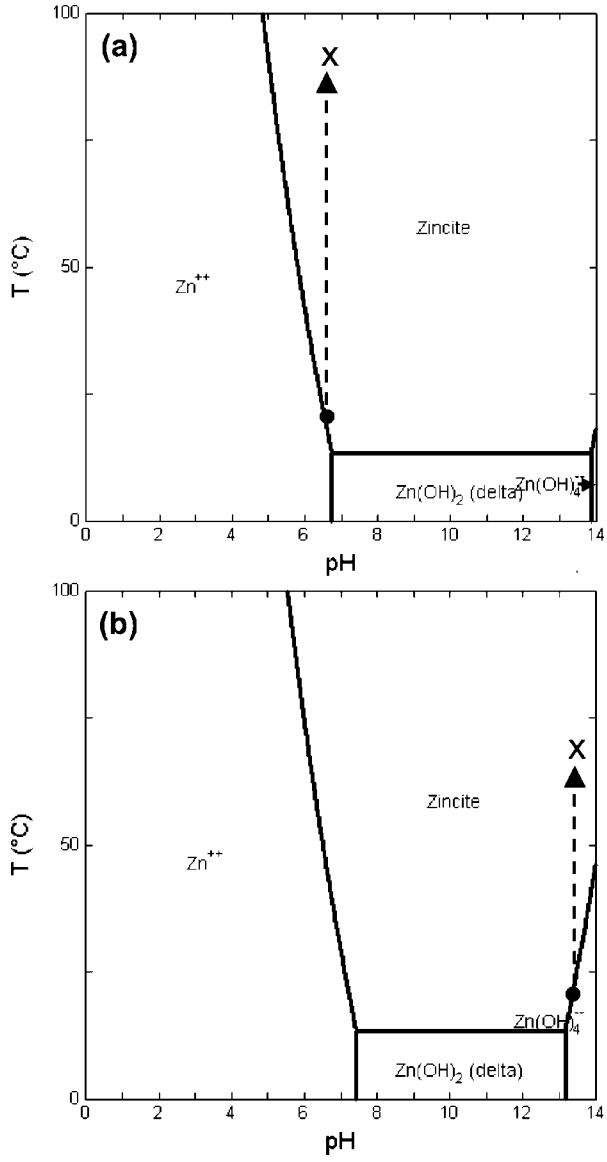

Figure 1. Speciation diagram of Zn as a function of pH and temperature in aqueous solutions containing Zn activity of (a) 25 mM (HMT recipe) and (b) 1 mM (NaOH recipe). The initial temperature is marked by the circle and the growth temperature is marked by the cross.

determined by X-ray diffractometry (XRD, Rigaku) with Cu Kα radiation. The average nanorod diameter was also approximated by the crystalline domain size calculated from ZnO (0002) peak using the Scherer equation $t = 0.9\,\lambda/(B\cos\theta)$, where t is the domain size, λ is the X-ray wavelength, and B is the angular fwhm of the peak at angle θ. Speciation diagrams were produced using Geochemist's Workbench (GWB Software, Golden, CO), which generates species distribution and stability diagrams versus activity based on the Minteq database of thermodynamic data.

Results and Discussion

Effect of Solution pH. We found that different growth solution pH values significantly altered the growth rate and morphology of ZnO NRAs on highly oriented ZnO seed layers. As shown by the zinc speciation diagrams for activities of 25 mM (Figure 1a) and 1 mM (Figure 1b), the growth solution is saturated at room temperature with Zn^{2+} for the HMT recipe and $Zn(OH)_4^{2-}$ for the NaOH recipe, respectively. As the solution is heated to the reaction temperature, denoted by a cross in Figure 1, the zincite (ZnO) phase becomes thermodynamically

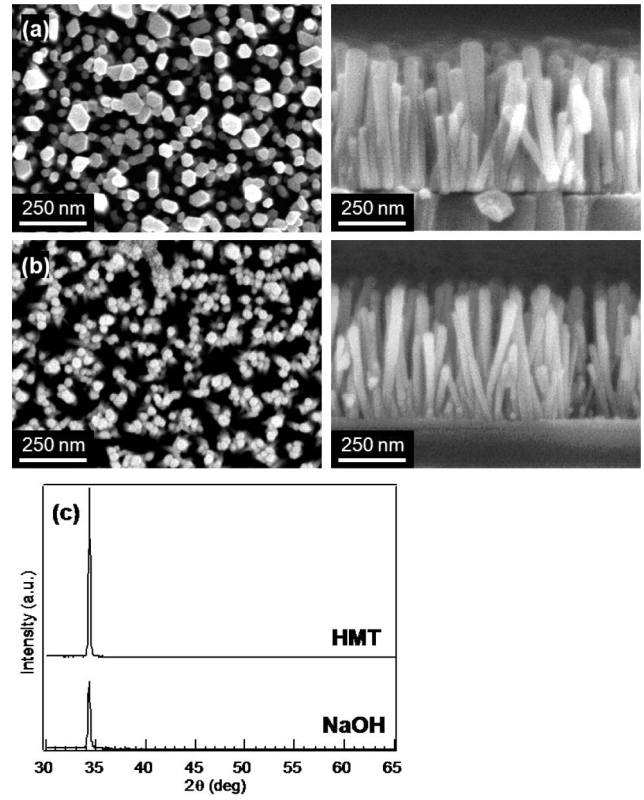

Figure 2. Comparison of ZnO NRAs of ~500 nm length grown in different pH solutions. (a) Plane view (left) and cross sectional (right) SEM of NRA via HMT recipe (pH ~ 6.8), growth time = 115 min. (b) Plane view (left) and cross sectional (right) SEM of NRA via NaOH recipe (pH ~ 13.2), growth time = 70 min. (c) XRD data of the NRAs via HMT (top) and NaOH (bottom) recipes.

favored, and the zinc ions react on the seed layer via hydrolysis and condensation to initiate nanorod growth. We should note that the HMT growth solution has a pH of ~6.8, while the same solution without HMT has a pH of ~5.5. Thus, by maintaining solution pH, HMT helps regulate the growth of ZnO. Despite using the same type of seed layer, significant differences in ZnO NRA morphology were observed between neutral and high pH growth solutions. For example, for NRAs of approximately equal length (500 nm), the NaOH recipe (Figure 2b) resulted in NRAs with average nanorod diameters of ~35 nm compared to ~50 nm for the HMT recipe (Figure 2a). XRD data indicate that both ZnO NRAs are highly aligned with only the ZnO (0002) peak present (Figure 2c). From the width of the peak, we determined the average minimum crystalline domain size, which also corresponds to the average nanorod diameter since each nanorod is a single crystal.[9] For NRAs of 500 nm length, we found a nanorod diameter of 47 and 34 nm grown using the HMT and the NaOH method, respectively, in good agreement with SEM data. Because of the smaller diameters, NRAs using the NaOH recipe occupied a smaller volume fraction than those grown by the HMT recipe, as evident in Figure 2b by the greater amount of space between the nanorods. The smaller volume fraction is consistent with the ratio of integrated XRD intensity for the ZnO (0002) peak for NaOH versus HMT recipe, which is ~0.6 (Figure 2c). The HMT recipe also yielded nanorods with well-defined $\{10\bar{1}0\}$ facets and hexagonal cross sections as shown in the plane view SEM image (Figure 2a). In contrast, the NaOH recipe results in nanorods that are much less faceted, with a rounded cross section (Figure 2b).

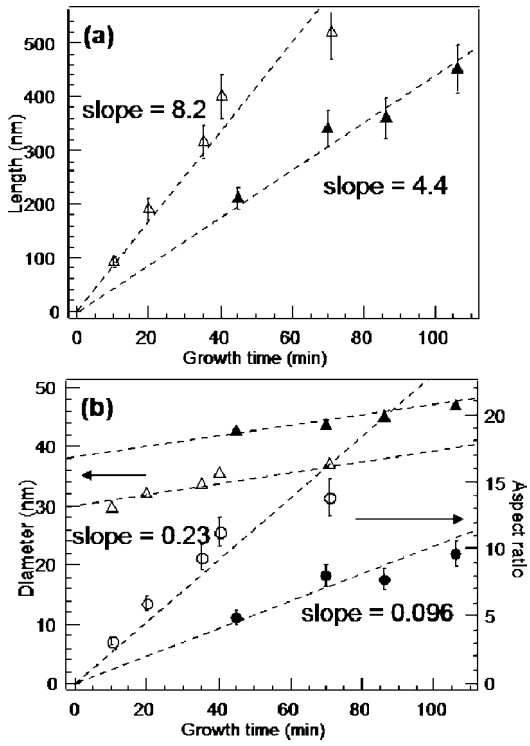

Figure 3. Dimensions of nanorods deposited on oriented ZnO using the HMT (closed symbols) and NaOH (open symbols) recipe. (a) Nanorod length from SEM versus growth time. Linear fit to length data (dashed) and growth rate (slope of linear fit) are also shown. (b) Diameter from XRD (triangles) and aspect ratio (circles) versus growth time. Linear fit to aspect ratio data (dashed) and slope are also shown. Dashed lines for diameter are guides to the eyes only because of nonzero intercept.

Comparison of ZnO NRAs dimensions as a function of growth time using HMT and NaOH recipes reveals additional information on ZnO nanorod growth dynamics. First, nanorod length linearly increased at a fitted rate of 8.2 nm/min for the NaOH recipe compared to 4.4 nm/min for the HMT recipe (Figure 3a), confirming that a high pH causes an increase in the absolute deposition rate on the ZnO (0001) surface. While nanorod diameter for the NaOH recipe is consistently smaller than that for the HMT recipe, the growth rate of nanorod diameter is similar for both recipes (Figure 3b, triangles). We also found that a linear fit of nanorod diameter versus growth time yielded positive intercepts for time = 0 (Figure 3b, triangles), which is also the case even if we take into account the time needed for the solution to reach the growth temperature (~20 min). This suggests that nanorod diameter increased rapidly during initial stages of growth for both recipes, in contrast to the linear growth in nanorod length. Plotting the nanorod aspect ratio as a function of growth time, we again found a faster linear increase of 0.23/min for the NaOH recipe versus 0.096/min for the HMT recipe (Figure 3b, circles), indicating that deposition on the (0001) surface is preferentially enhanced over the $\{10\bar{1}0\}$ surfaces. These results can be explained by the different charge on the zinc ions for HMT and NaOH recipe, which are Zn^{2+} and $Zn(OH)_4^{2-}$, respectively (Figure 1). Because the ZnO (0001) surface is positively charged,[23] the negatively charged $Zn(OH)_4^{2-}$ may be preferentially attracted to the growth facet. In contrast, since the $\{10\bar{1}0\}$ surfaces are uncharged, no significant difference in the diameter growth rate is expected. In short, high solution pH preferentially enhanced growth of ZnO NRAs along the <0001> direction both in absolute magnitude and also in comparison to other crystallographic directions, possibly due to attractive interactions between $Zn(OH)_4^{2-}$ ions and the positively charged Zn terminated (0001) surface. As a result, a shorter growth time is required for the deposition of ZnO NRAs of a given length using the NaOH recipe, leading to smaller nanorod diameter, poor faceting, and lower NRA volume fraction.

Effect of DAP Concentration. DAP mediates the growth of ZnO nanoneedles in a qualitatively similar fashion on the three seed layers that we examined. However, the concentration range at which the mediation occurs and the morphology and alignment of the deposited nanoneedles differ between seed layer types. It should be noted that since DAP is a base, the growth solution pH increased with the addition of DAP, from ~10 at [DAP] = 43 mM to ~12 at [DAP] = 190 mM. Although the speciation diagrams in Figure 1 suggest that zinc is normally not soluble over these pH ranges at room temperature, we found the growth solution to be transparent for [DAP] > 43 mM due to the formation of soluble zinc−amino complex.[21,22] When we compared ZnO deposition in the presence of DAP on three seed layers, we noticed two major effects. First, in contrast to the NaOH recipe where only the pH was adjusted, solutions containing DAP resulted in nanorods with tapered tips, or nanoneedles, and the extent of the tapered region became longer at higher [DAP] (Figure 4a,b). We previously proposed that the tapering may be caused by reversible adsorption of DAP to the (0001) facet of ZnO during growth, which retards Ostwald ripening and preserves minute (0001) steps to create the tapered tip profile.[21]

Second, the seed layer strongly influenced ZnO volume fraction and alignment of the NNAs. For example, an oriented ZnO seed layer yielded close packed, highly aligned ZnO NNAs at all [DAP] (Figure 4a). The densely packed seed layer with the (0001) growth facet oriented parallel to the substrate[9] allowed for unimpeded growth of the nanoneedles, thus maximizing alignment and NNA volume fraction. In contrast, a nanoparticle seed layer led to less aligned ZnO NNAs with decreasing volume fraction at increasing [DAP] (Figure 4b). Because of the random orientation of the (0001) facet on the nanoparticles with respect to the substrate, the ZnO nanoneedles grew in random directions, causing many to impinge on the substrate or other nanoneedles, which terminated growth and decreased NNA volume fraction. On a seed layer of ZnO microrods, the nanoneedles grew primarily on the $\{10\bar{1}0\}$ facets of the microrods, and the nanoneedle *c*-axis were oriented at ~80° to the microrod *c*-axis for all [DAP] due to an energetically favored twin configuration.[21] The packing density of the ZnO branch arrays was independent of [DAP] up to [DAP] ~ 125 mM (Figure 4c), at which point the volume fraction diminished sharply with [DAP]. Previously we showed that DAP caused the nucleation of a layer of polycrystalline ZnO on the microrod to act as the seed layer, but for [DAP] > 125 mM, the level of zinc supersaturation was too low to overcome the free energy of nucleation of seeds on the $\{10\bar{1}0\}$ surfaces, so no nuclei were formed.[21,22] Thus, at [DAP] = 125 mM, nucleation was slow and sparse on the microrod surface, and for [DAP] > 125 mM no needle growth was observed.

When the characteristic dimensions of the nanoneedle arrays for the three types of substrates were extracted from SEM images, their dependence on [DAP] and seed layer type became apparent. On oriented ZnO film and ZnO microrod seed layers, the average nanoneedle length increased with [DAP] at different rates and reached maximum values of 3.65 and 8.9 μm, respectively, at [DAP] = 125 mM after 18 h (Figure 5a). In

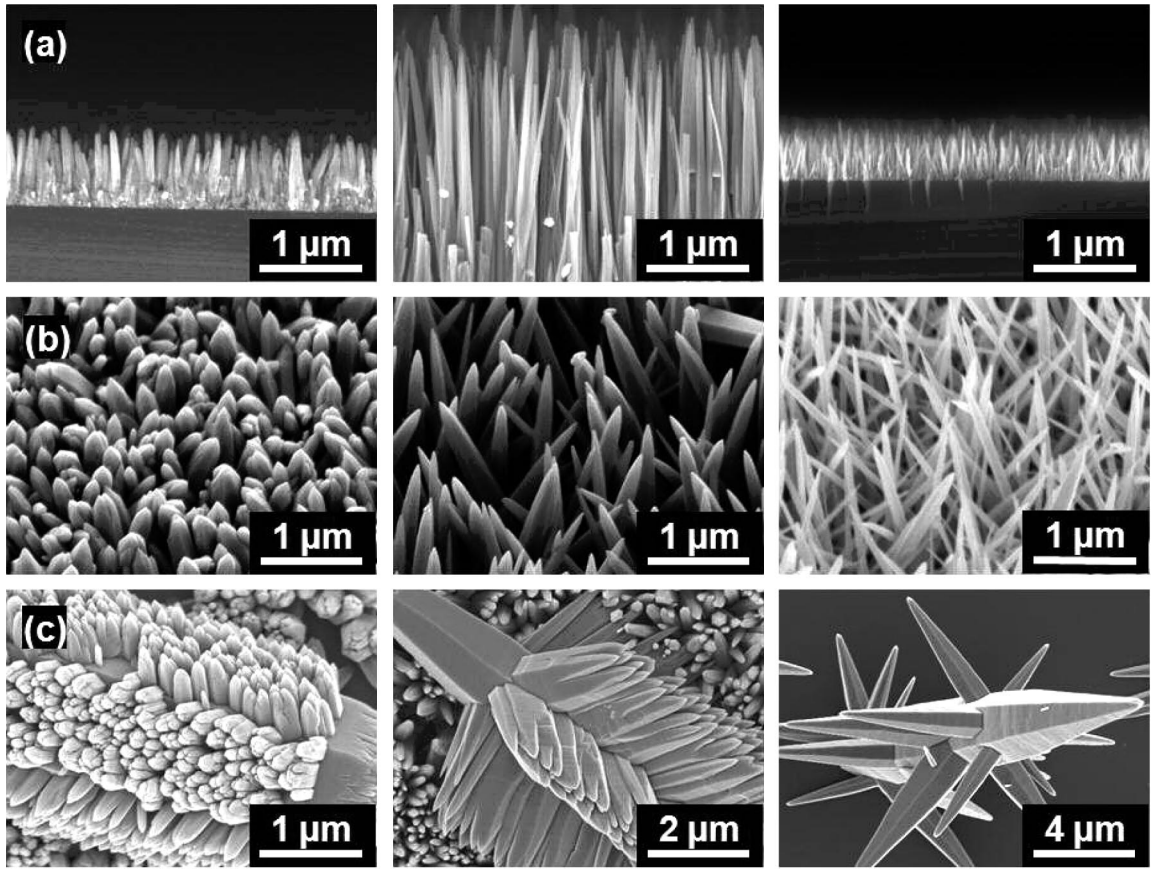

Figure 4. Comparison of ZnO nanoneedle arrays grown at different [DAP] on three seed layers. (a) Cross sectional view on oriented ZnO film; from left, 40 mM, 125 mM, 190 mM. (b) 40° tilt view on ZnO nanoparticles; from left, 40 mM, 125 mM, 190 mM. (c) Plane view on ZnO microrods; from left, 40 mM, 80 mM, 125 mM. No branch growth was observed at [DAP] > 125 mM.

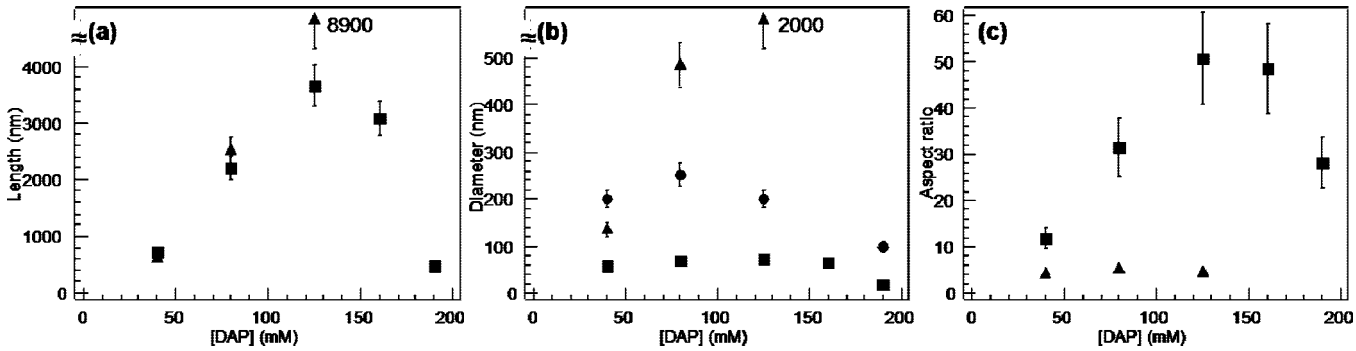

Figure 5. Dimensions of NNAs deposited on oriented ZnO film (squares), ZnO microrods (triangles), and ZnO nanoparticles (circles) under identical growth conditions for 18 h as a function of DAP concentration. (a) Length. (b) Diameter. (c) Aspect ratio. Average nanoneedle length and aspect ratio were not determined for NNAs on nanoparticles due to low degree of orientation.

addition, a ZnO NNA on microrods exhibited a consistently larger length compared to an NNA on oriented ZnO film at the same [DAP]. For [DAP] > 125 mM, the average nanoneedle length decreased on oriented ZnO films, and no ZnO nanoneedles were observed on ZnO microrods due to a lack of nucleation sites, as previously mentioned. In contrast, the average nanoneedle length on ZnO nanoparticles continued to increase as [DAP] increased above 125 mM (Figure 4b), although we could not quantitatively measure the length due to the random alignment of the nanoneedles. The average nanoneedle diameter on all three seed layer types increased as a function of [DAP] until maximum values were reached at [DAP] = 80 to 125 mM. At higher [DAP], the average nanoneedle diameter decreased for NNAs on oriented ZnO films (Figure 5b, squares) and ZnO nanoparticles (Figure 5b, circles), and became zero on ZnO microrods as new ZnO crystals did not nucleate. For a ZnO NNA on oriented ZnO film at [DAP] = 190 mM, we found an average nanoneedle diameter of 17 nm, which is the smallest value that we know of using nonhydrothermal aqueous growth. Comparing the average nanoneedle diameter for the three seed layers at the same [DAP], we again found that an oriented ZnO film generally yielded the smallest diameter, followed by nanoparticles and then by microrods. Finally, NNAs on microrods exhibited a constant aspect ratio of ~4.5 for all [DAP] (Figure 5c, triangles), whereas NNAs on oriented ZnO films exhibited various aspect ratios with a maximum value of ~50 at [DAP] = 125 mM (Figure 5c, squares).

The trend in nanoneedle dimensions versus [DAP] may be explained by the following combination of factors. First, chelation by DAP decreases supersaturation of zinc ions, which tends to decrease the growth rate of ZnO nanoneedles. However, it also enhances heterogeneous versus homogeneous growth, as seen by the fact that growth solutions with [DAP] ≥ 80 mM contained no ZnO precipitate which nucleated homogeneously from solution. As a result, ZnO may be preferentially deposited on the nanoneedles at [DAP] ≤ 125 mM, leading to increased growth rate for both length and diameter. In contrast, at [DAP] > 125 mM, the additional chelation may decrease supersaturation sufficiently to hinder the growth of ZnO nanoneedles.

Second, due to differences in orientation and surface coverage between seed layers, the areal density of viable nuclei, that is, those which led to full length nanoneedles, was highest for oriented ZnO film, followed by nanoparticles and finally the sparsely coated ZnO microrods. Since the zinc content was constant for all growth solution and the growth time of 18 h was sufficiently long to carry the reaction to completion,[22] it is reasonable that the dimensions per nanoneedle were generally smallest on oriented ZnO film (Figure 5a,b, squares) and largest on ZnO microrods (Figure 5a,b, triangles). In addition, the lower viable nuclei density on ZnO nanoparticles compared to oriented ZnO film may decrease the amount of ZnO deposited from solution per unit time so that the ZnO nanoneedles grow in the [0001] direction for a longer period of time before the zinc concentration falls below the supersaturation limit. This may explain the continued increase in nanoneedle length versus [DAP] on nanoparticle seed layers (Figure 4b). Finally, ZnO nanoneedles on microrods were shown to coalesce during growth into larger nanoneedles in the presence of DAP,[22] which further explains their larger dimensions (Figures 5a,b, triangles) and increased spacing between nanoneedles (Figure 4c) as [DAP] increases. Coalescence does not appear to occur for ZnO NNAs deposited on oriented ZnO film and on ZnO nanoparticles, possibly because each nanoneedle grows from a discrete nanocrystal, which is not perfectly aligned with the other nanocrystal seeds.

Conclusions

We demonstrated that the dimensions and morphology of ZnO nanorods arrays and nanoneedle arrays can be controlled by varying growth solution pH and DAP concentration on different types of seed layers. Increasing the growth solution pH from near neutral to highly basic conditions using NaOH resulted in increased deposition on the (0001) surface and reduced deposition on and faceting of the $\{10\bar{1}0\}$ surfaces, possibly due to favorable interactions between $Zn(OH)_4^{2-}$ ions at high pH and the positively charged (0001) surface. Increasing the DAP concentration from 43 to 190 mM created NNAs with more pronounced tip tapering, while nanoneedle length and diameter reached their maximum values at [DAP] ∼ 125 mM. Further increases in DAP concentration decreased the nanoneedle diameter while varying the nanoneedle length in a complex fashion depending on the seed layer. The aspect ratio of NNAs on oriented ZnO film reached a maximum of ∼50 at [DAP] = 125 mM, whereas the aspect ratio on ZnO microrods remained constant at ∼4.5. We explain the trends in nanoneedle dimensions, alignment, and volume fraction via a combination of zinc chelation by DAP, interplay between the finite zinc supply in solution and the number density ZnO nanoneedles on different seed layers, and details in nucleation and coalescence of ZnO nanoneedles on microrod seed layers. With an improved understanding of the relationship between growth conditions and resulting morphology of the ZnO nanostructures, we will be able to optimize ZnO nanostructures for specific applications.

Acknowledgment. We thank M. Piech for assistance with ZnO nanoneedle array synthesis, and N. Bell for calculating the speciation diagrams. This project is financially supported by the Laboratory Directed Research and Development program at Sandia. Sandia is a multiprogram laboratory operated by Sandia Corporation, a Lockheed Martin Company, for the United States Department of Energy under contract DE-AC04-94AL85000.

References

(1) Huang, M. H.; Mao, S.; Feick, H; Yan, H.; Wu, Y.; Kind, H.; Weber, E.; Russo, R.; Yang, P. *Science* **2001**, *292*, 1897.
(2) Konenkamp, R.; Dloczik, L.; Ernst, K.; Olecsh, C. *Physica E* **2002**, *14*, 219.
(3) Yamamoto, T.; Shiosaki, T.; Kawabata, A. *J. Appl. Phys.* **1980**, *51*, 3113.
(4) Wang, Z. L.; Song, J. *Science* **2006**, *312*, 242.
(5) Look, D. C. *Mater. Sci. Eng., B* **2001**, *80*, 383.
(6) Yang, P.; Yan, H. Q.; Mao, S.; Russo, R.; Johnson, J.; Saykally, R.; Morris, N.; Pham, J.; He, R. R.; Choi, H. J. *Adv. Funct. Mater.* **2002**, *12*, 323.
(7) Vayssieres, L.; Keis, K.; Lindquist, S.-E.; Hagfeldt, A. *J. Phys. Chem. B.* **2001**, *105*, 3350.
(8) Greene, L. E.; Law, M.; Goldberger, J.; Kim, F.; Johnson, J. C.; Zhang, Y.; Saykally, R. J.; Yang, P. *Angew. Chem., Int. Ed.* **2003**, *42*, 3031.
(9) Greene, L. E.; Law, M.; Tan, D. H.; Montano, M.; Goldberger, J.; Somorjai, G.; Yang, P. *Nano Lett.* **2005**, *5*, 1231.
(10) Govender, K.; Boyle, D. S; Kenway, P. B; O'Brien, P. *J. Mater. Chem.* **2004**, *14*, 2575.
(11) Lee, Y.-J.; Sounart, T. L.; Scrymgeour, D. A.; Voigt, J. A.; Hsu, J. W. *J. Cryst. Growth* **2007**, *304*, 80.
(12) Hsu, J. W. P.; Tian, Z. R.; Simmons, N. C.; Matzke, C. M.; Voigt, J. A.; Liu, J. *Nano Lett.* **2005**, *5*, 83.
(13) Hsiao, C.-S.; Peng, C.-H.; Chen, S.-Y. *J. Vac. Sci. Technol. B* **2006**, *24*, 288.
(14) Gui, Z.; Wang, X.; Liu, J.; Yan, S.; Ding, Y.; Wang, Z.; Hu, Y. *J. Solid State Chem.* **2006**, *179*, 1984.
(15) Tak, Y.; Yong, K. *J. Phys. Chem. B* **2005**, *109*, 19263.
(16) Xu, F.; Yuan, Z.-Y.; Du, G.-H.; Ren, T.-Z.; Bouvy, C.; Halasa, M.; Su, B.-L. *Nanotechnology* **2006**, *17*, 588.
(17) Peterson, R. B.; Fields, C. L.; Gregg, B. A. *Langmuir* **2004**, *20*, 5114.
(18) Cui, J.; Gibson, U. J. *J. Phys. Chem. B* **2005**, *109*, 2207.
(19) Scrymgeour, D. A.; Sounart, T. L.; Simmons, N. C.; Hsu, J. W. P. *J. Appl. Phys.* **2007**, *101*, 014316.
(20) Tian, Z. R.; Voigt, J. A.; Liu, J.; McKenzie, B. B.; McDermott, M. J.; Rodriguez, M. A.; Konishi, H.; Xu, H. *Nat. Mat.* **2003**, *2*, 821.
(21) Sounart, T. L.; Liu, J.; Voigt, J. A.; Hsu, J. W. P.; Spoerke, E. D.; Tian, Z. R.; Jiang, Y. *Adv. Funct. Mat.* **2006**, *16*, 335.
(22) Sounart, T. L.; Liu, J.; Voigt, J. A.; Huo, M.; Spoerke, E. D.; McKenzie, B. B. *J. Am. Chem. Soc.* **2007**, *129*, 15786–15793.
(23) Gao, P. X.; Wang, Z. L. *J. Appl. Phys.* **2005**, *97*, 044304.

CG800052P